

Monte Carlo Simulation of the Galactic ^{26}Al Gamma-Ray Map

Eric J. Lentz, David Branch, and E. Baron

Department of Physics and Astronomy, University of Oklahoma, 440 W. Brooks, Norman,
OK 73019-0225

lentz,branch,baron@mail.nhn.ou.edu

ABSTRACT

The observed map of 1.809 MeV gamma-rays from radioactive ^{26}Al (Oberlack et al, 1996) shows clear evidence of a Galactic plane origin with an uneven distribution. We have simulated the map using a Monte Carlo technique together with simple assumptions about the spatial distributions and yields of ^{26}Al sources (clustered core-collapse supernovae and Wolf Rayet stars; low- and high-mass AGB stars; and novae). Although observed structures (e.g., tangents to spiral arms, bars, and known star-forming regions) are not included in the model, our simulated gamma-ray distribution bears resemblance to the observed distribution. The major difference is that the model distribution has a strong smooth background along the Galactic plane from distant sources in the disk of the Galaxy. We suggest that the smooth background is to be expected, and probably has been suppressed by background subtraction in the observed map. We have also found an upper limit of $1M_{\odot}$ to the contribution of flux from low-yield, smoothly distributed sources (low-mass AGB stars and novae).

Subject headings: gamma rays: theory—nuclear reactions, nucleosynthesis, abundances –Galaxy: abundances

1. Introduction

The gamma-ray created by the decay of ^{26}Al to ^{26}Mg was the first discovered Galactic gamma-ray line (Mahoney et al 1982). The ^{26}Al nucleus decays by positron emission to the first excited state of ^{26}Mg , which subsequently decays to the ground state emitting a 1.809 MeV gamma-ray. The mean lifetime of ^{26}Al , $\tau = 1.05 \times 10^6$ years, makes the 1.809 MeV gamma ray line an excellent tracer for newly synthesized material released into the ISM over the last several million years.

The main production mechanism of ^{26}Al is proton capture on ^{25}Mg . Astrophysical environments that can produce ^{26}Al include hydrostatic H-burning in the convective cores of massive stars and the H-burning shells of intermediate mass stars, and explosive H burning in novae. The carbon and neon rich shells of massive stars are also a site for ^{26}Al production both statically and explosively. In addition to its production, the fresh ^{26}Al must be transported into the ISM before it decays in order to be observable. The explosive mechanisms present no problems, but the transport timescale in AGB stars is of similar order to the decay timescale causing a reduction in the amount of ^{26}Al released into the ISM.

The first map of Galactic 1.809 MeV gamma-ray emission from ^{26}Al was published by Oberlack et al (1996) from COMPTEL data. This map has a 1σ angular resolution of 1.6° , or 3.8° FWHM. The map was produced using a Maximum-Entropy method after background subtraction. The 1.809 MeV gamma-ray map has several important characteristics, including the concentration of emission in the Galactic plane, a strong, irregular emission region toward the inner Galaxy, and a generally uneven, or clumpy, emission distribution. Along the Galactic plane there are several disconnected emission regions, some of which have been associated with O-B associations, spiral arm tangents, and the Vela SNR. Chen et al (1996) also identify several of the regions with spiral arm tangents. A recent and thorough review of the entire topic including observation, sources, and distribution of ^{26}Al can be found in Prantzos and Diehl (1996).

These observations can best be explained with sources that are spatially concentrated and rare. If the major sources of emission had small yields and a smooth Galactic distribution, the emission would be quite uniform. This is not seen in the published results (Oberlack et al 1996), which show large gaps along the Galactic plane between emission regions. We have therefore built a Monte Carlo model for the Galactic ^{26}Al emission containing all potential astronomical sources. We have also allowed the most massive stars to form clusters that do not dissociate in the lifetime of those stars. We have made only the simplest of assumptions about Galactic structure, an exponential disk and a bulge. We have not attempted to represent any specific observed structures in the Galaxy. All non-uniformities arise from the random nature of the simulation. This produces a map that, to the eye, has a strong resemblance to the observations, with the exception of a persistent uniform background not found in the reduced observational data.

We plan to use more statistically rigorous methods to measure the strength of this similarity in future work, as well as to consider some of the effects of non-uniform structure and the enhanced resolution of the INTEGRAL observatory.

2. Model

Our model of Galactic ^{26}Al 1.809 MeV gamma-ray flux uses a Monte Carlo model of the Galaxy to generate the raw flux data (§ 2.1), and a gaussian smoothing technique to plot the data on an equal-area projection of the sky (§ 2.2).

2.1. Monte Carlo Model

We have modified the Monte Carlo model of the Galaxy developed by Hatano, Fisher & Branch (1997a) to study supernova visibility. The data are generated as a series of point source events. For each point in the disk the radial and vertical positions are drawn from exponential distributions. Each point in the bulge is drawn from the distribution $(R^3 + a^3)^{-1}$, where R is the distance to the Galactic center and $a = 0.7$ kpc. The age of the event is selected uniformly from a fixed simulation length. The ^{26}Al yield of each event is reduced to account for the radioactive decay and the current decay rate is computed to give the current gamma-ray luminosity. The luminosity is geometrically diluted to compute the flux at the Earth. The data are saved individually or in bins smaller than the detector resolution ($\frac{1}{8}^\circ$ vs. 1.6°).

The computation of the flux from clusters of massive stars requires additional steps. Each star cluster is assigned a random size and age. The age of the clusters is drawn from a span which is longer than the simulation length by the evolutionary timescale of the slowest evolving constituent star. With the assumption of coeval star formation, this allows the stellar death rates to be in equilibrium across the simulation length. The mass of each star in a cluster is drawn from a power-law initial mass function (IMF) of the form $f(m) \propto m^{-2.7}$. The mass of the star will determine the evolutionary timescale and yield of the subsequent supernova. The age of each contributing event is computed by subtracting the evolutionary timescale from the age of the cluster. Stars that have not yet reached the end of their evolutionary tracks are removed from the simulation. The ^{26}Al gamma-ray fluxes are computed from the yields as described above. If the star is a Wolf-Rayet progenitor, the appropriate ^{26}Al yield will be added at a fixed time before the end of stellar evolution. The values of the yields, scales, etc. will be given in the section describing the simulation (§ 3).

2.2. Flux Mapping Method

We have also developed a procedure to translate the randomly placed data points into an intensity map. The data generated in § 2.1 were first sorted into bins one degree on each side to speed later calculations. To compute the local intensity at any point, the flux from each point within a circular window of fixed radius was summed using a Gaussian weight dependent on the distance between the data point and evaluation point. The radius of the fixed circle was chosen to be three times the smoothing length or Gaussian width, σ . This value was found to be good to about 0.1% by simple tests with centrally peaked and flat test functions. All distances were computed in degrees of arc, and the data bins that were used to compute each flux point were carefully selected to cover the entire area of the circular window. The local flux was computed at one degree intervals in Galactic coordinates, and plotted with contours of $1.57 \times 10^{-5} \gamma \text{ cm}^{-2} \text{ s}^{-1}$ in Figure 1.¹

3. The Simulation

In constructing our model of the Galaxy we have chosen a bulge with radius 3 kpc, and a disk that extends to a radius of 20 kpc with a radial scale length of 5 kpc. The Earth is placed in the Galactic plane at a radius of 8 kpc. Objects with low-mass progenitors, (novae, AGB stars), have a disk component that extends to the center of the Galaxy with a vertical scale height of 350 pc. The low-mass AGB stars and novae also have a bulge component with a 7:1 disk-to-bulge ratio as per the nova implementation of the same model (Hatano et al 1997b). High-mass objects (SN, W-R) consist only of a disk component with a 50 pc scale height that does not include the inner 3 kpc of the Galaxy where the bulge is located. Additionally, the high-mass objects are clustered into groups of $10 \pm 2\sigma$ stars, where σ is four.

3.1. Source Frequencies

To compute the rate of the component sources in the model we have followed the analysis of Prantzos and Diehl (1996) on the rate of ²⁶Al production. We therefore choose an initial mass function of $f(m) \propto m^{-2.7}$ for progenitors with $M > 1M_{\odot}$, and a star formation rate of $\sim 5 \text{ stars yr}^{-1}$. We also refer to AGB stars with 1–4 M_{\odot} progenitors as low-mass and those with 4–9 M_{\odot} progenitors as high-mass. Supernova and Wolf-Rayet

¹Plots made using routines from the PGLOT Graphics Subroutine Library by T. J. Pearson.

progenitors will be those stars from $9 M_{\odot}$ up to $120 M_{\odot}$. For novae we have adopted the value 40 yr^{-1} suggested by Hatano et al (1997b) using the same model geometry. Table 1 summarizes the rates, yields, and model fluxes for the ^{26}Al sources used to make Figure 1.

3.2. ^{26}Al Yields

The yields of Weaver and Woosley (1993) are used for supernovae. These models use a large grid of nuclei, to give more accurate results in the synthesis of various isotopes, in the pre-supernova phase and the explosive phase. The yields of Meynet et al (1997) are used for Wolf-Rayet phase sources. These models also use an expanded network of nuclear reactions to cover the MgAl chain. Models were calculated for three metallicities, $Z = 0.008, 0.020, 0.040$. Our model Galaxy includes three radial zones, with inner radii of 12 kpc, 6 kpc, and 3 kpc respectively for the three metallicities. AGB stars are divided into low- and high-mass with the division at $4 M_{\odot}$ as in Prantzos and Deihl (1996). We follow their use of $3 \times 10^{-5} M_{\odot}$ ^{26}Al per high-mass AGB star from Bazan et al (1993) and $10^{-8} M_{\odot}$ ^{26}Al per low-mass AGB star from Forestini, Paulus, & Arnould (1991). For novae we use $5 \times 10^{-10} M_{\odot}$ ^{26}Al for CO novae and $8 \times 10^{-9} M_{\odot}$ ^{26}Al for ONe novae from the models of José, Hernanz, and Coc (1997). We discuss a limit to the smooth source contribution in § 4.1.

3.3. Best Model

Combining the sources in with the self-consistent frequencies in § 3.1 and the yields in § 3.2 gives the map in Figure 1 using the same contours as in Oberlack et al (1996) for comparison. Figures 2a,b,c are the smooth (novae and low-mass AGB stars plotted with contours one-tenth the standard value), high-mass AGB star, and massive star (W-R and SNe) components respectively, used to make Figure 1 using the same contours. We see that high-mass AGB stars provide some of the irregularity seen in the observations and that massive star sources provide the concentration of flux from the inner region of the Galaxy, $|\ell| < 30^{\circ}$. The SNe/W-R component provides most of the observed irregularity. The smooth, low-yield component (novae and low-mass AGB stars) does not make a detectable contribution in this simulation. The extent to which larger contributions can be made by these sources without distorting the results in Figure 1 is given in § 4.1. The total flux from each sub-component can be found in Table 1. The component contributions are $0.12 M_{\odot}$ ^{26}Al from the smooth component, $0.93 M_{\odot}$ ^{26}Al from high-mass AGB stars, and $0.76 M_{\odot}$ ^{26}Al from massive stars.

3.4. Detectability

For a point source the 3σ detection flux for narrow lines at 1.8 MeV with COMPTEL, $F_{3\sigma}$, is $3 \times 10^{-5} \gamma \text{ cm}^{-2}$ (Schönfelder et al 1993) for a 10^6 second exposure. When incorporated with the Gaussian smoothing kernel (instrument response function) of $\sigma = 1.6^\circ$ the 3σ intensity limit, $I_{3\sigma}$, is $6 \times 10^{-3} \gamma \text{ cm}^{-2} \text{ s}^{-1} \text{ sr}^{-1}$ for a 10^6 second exposure. The data used in Oberlack et al (1996) represents 3.5 years of COMPTEL observations with exposures along the Galactic plane from ~ 35 - 55×10^6 seconds. We have chosen 45×10^6 seconds as the representative exposure time for the simulated map. Using this exposure, the 1σ detection limit, $I_{1\sigma}$, is $3 \times 10^{-4} \gamma \text{ cm}^{-2} \text{ s}^{-1} \text{ sr}^{-1}$. This is about twice the contour interval used in the map of Oberlack et al (1996) and in Figures 1&2. These contours then approximately represent one-half sigma confidence contours.

4. Comparison with Observations

The main goal of this paper is to reproduce the “look and feel” of the observed intensity map of Oberlack et al (1996). It should be noted that we have made no attempt to reproduce individual features of the observations by placing individual sources and clusters in specific places. Such an approach would lead to an artificial reproduction of the observation by introducing too many free parameters.

Like the observations, the central region of the simulation, Figure 1, the inner $\pm 30^\circ$ shows a strong region of emission closely restrained to the Galactic plane with internal irregularities. As in the observations, the central emission region ends rapidly 30° from the Galactic Center. Disconnected peaks and emission regions along the Galactic plane outside of the inner Galaxy appear in both observation and simulation.

The main difference between the simulation and observation is the presence of an extended background along the Galactic plane at the level of the first plotted contour in the simulation. As noted in § 3.4, the first plotted contour is roughly equivalent to one-half sigma confidence. We suspect that the complex and difficult extraction of the 1.8 MeV gamma-line map from the significant background has resulted in the disappearance of the low-level background. We also suspected the maximum entropy method (MEM) may be responsible for suppressing the low-level background, but the application of MEM to the simulated data did not cause the low-level background to disappear. This leads us to suspect that the background subtraction is the likely cause for the disappearance of the low-level background from the observations.

Only points within the second contour in our simulations would have even a 2/3 chance

of being observed in the current COMPTEL data. We suggest that with the sensitivity to see $10^{-4} \gamma \text{ cm}^{-2} \text{ s}^{-1} \text{ sr}^{-1}$ intensities with 1σ confidence or better, about 400×10^6 seconds of exposure, a low-level background along the plane from distant and indistinguishable sources would be inevitably found.

4.1. Limit on Smoothly Distributed Sources

The “smooth” component, low-mass AGB’s and novae (Figure 2a), contains about $1/8 M_{\odot}$ of ^{26}Al which emits about $5 \times 10^{-5} \gamma \text{ cm}^{-2} \text{ s}^{-1}$, or about 1% of the total flux. We have tested how much of this smooth component can be added to the remaining sources without distorting the sum from the best model (Figure 1) to something incompatible with the map in Oberlack et al (1996). We have produced three models shown in Figures 3a,b,c that contain 4, 8, and 12 times the smooth component of our regular model respectively. The 4-fold model (Figure 3a, $0.5 M_{\odot} \text{ }^{26}\text{Al}$) has only minute differences from Figure 1, that require the two plots to be overlaid to be seen. The 8-fold model (Figure 3b, $1 M_{\odot} \text{ }^{26}\text{Al}$) shows a thickening of the inner Galaxy emission region and a small extension of the 1σ (second contour) background outside the inner Galaxy which is acceptable, but near the limit where it would be detectable with the current observations. The last model, Figure 3c with $1.5 M_{\odot} \text{ }^{26}\text{Al}$, shows considerable thickening of the inner Galaxy emission and an unacceptably long extension of Galactic plane background at the 1σ detection level. If such a large background were present, the Oberlack et al (1996) analysis should have shown stronger evidence of its existence. Therefore despite uncertainties in yields and rates for all objects, about $0.5 M_{\odot} \text{ }^{26}\text{Al}$ can be easily hidden in the smooth background without detection or modifying the results of this simulation, with an upper limit of about $1.0 M_{\odot} \text{ }^{26}\text{Al}$ in the smooth background.

5. Conclusions

Our simulation has shown that as expected by previous authors (e.g., Prantzos & Diehl, 1996), the sources with massive progenitors make most of the flux and provide the irregular structure seen in the observed map (Oberlack et al 1996). We have found that a background of strong sources diluted by distance should be detectable, with a longer exposure time. While the source rates and yields are uncertain we can limit the amount of ^{26}Al generated by the frequent but small ‘smooth’ sources to be about $1.0 M_{\odot}$. The total mass of ^{26}Al for the high-yield, massive progenitor sources is about $1.7 M_{\odot}$. This model produces a reasonable approximation of observation. The rates and yields of the massive

progenitor sources are also uncertain, but changes in yields can be compensated for by changes in rates as long as the number of distinct emission sites (clusters or high-mass AGB stars) does not change by a large factor.

This paper uses a Monte Carlo code of the Galaxy derived from the original version written by Adam Fisher. This work has been supported in part by NSF grants AST 9417102 and 9417242 and NASA grant NAG5-3505.

Table 1. Sources of ^{26}Al in Model.

Source	Rate (cen^{-1})	Yield (M_{\odot})	Model Flux ($\gamma \text{ cm}^{-2} \text{ s}^{-1}$)	
Novae (CO)	2800	5×10^{-10}	3×10^{-7}	bulge
			6×10^{-6}	disk
Novae (ONe)	1200	8×10^{-9}	2×10^{-6}	bulge
			4×10^{-5}	disk
Low-Mass AGB	40	10^{-8}	10^{-7}	bulge
			2×10^{-6}	disk
High-Mass AGB	3	3×10^{-5}	5×10^{-4}	
Massive Stars			3.2×10^{-3}	
Supernovae	1	10^{-5} to 10^{-4}		
Wolf-Rayet [†]		10^{-5} to 10^{-3}		

[†]Wolf-Rayet rate appropriate to related supernova progenitor

REFERENCES

- Bazan, G., Brown, L. E., Clayton, D.D., El , M. F., Hartmann, D. H., & Truran, J. W. 1993 in Compton Gamma-Ray Observatory, eds. M. Friedlander, N. Gehrels & D. Macomb (New York: AIP), 47
- Chen, W., Gehrels, N., Diehl, R., & Hartmann, D. 1996, A&AS, 120, 315
- Forestini, M., Paulus, G., & Arnould, M. 1991, A&A, 252, 597
- Hatano, K., Fisher, A., & Branch, D. 1997a, MNRAS, 290, 360
- Hatano, K., Branch, D., Fisher, A., & Starrfield, S. 1997b, MNRAS, 290, 113
- José, J., Hernanz, M., & Coc, A. 1997, ApJL, 479, L55
- Kolb, U., & Politano, M. 1997, A&A, 319, 909
- Mahoney, W. A., Ling, J.C., Jacobson, A. S., & Lingenfelter, R. 1982, ApJ, 262, 742
- Meynet, G., Arnould, M., Prantzos, N., & Paulus, G. 1997, A&A, 320, 460
- Oberlack, U., Bennett, K., Bloemen, H., Diehl, R., Dupraz, C., Hermsen, W., Knödlseher, J., Morris, D., Schönfelder, V., Strong, A., & Winkler, C. 1996, A&AS, 120, 311
- Prantzos, N. and Diehl, R. 1996, Physics Reports, 267, 1
- Schaller, G., Schaerer, D., Meynet, G., & Maeder, A. 1992, A&AS, 96, 269
- Schönfelder, V., et al. 1993, ApJS, 86, 657
- Weaver, T. A. & Woosley, S. E. 1993, Physics Reports, 227, 65

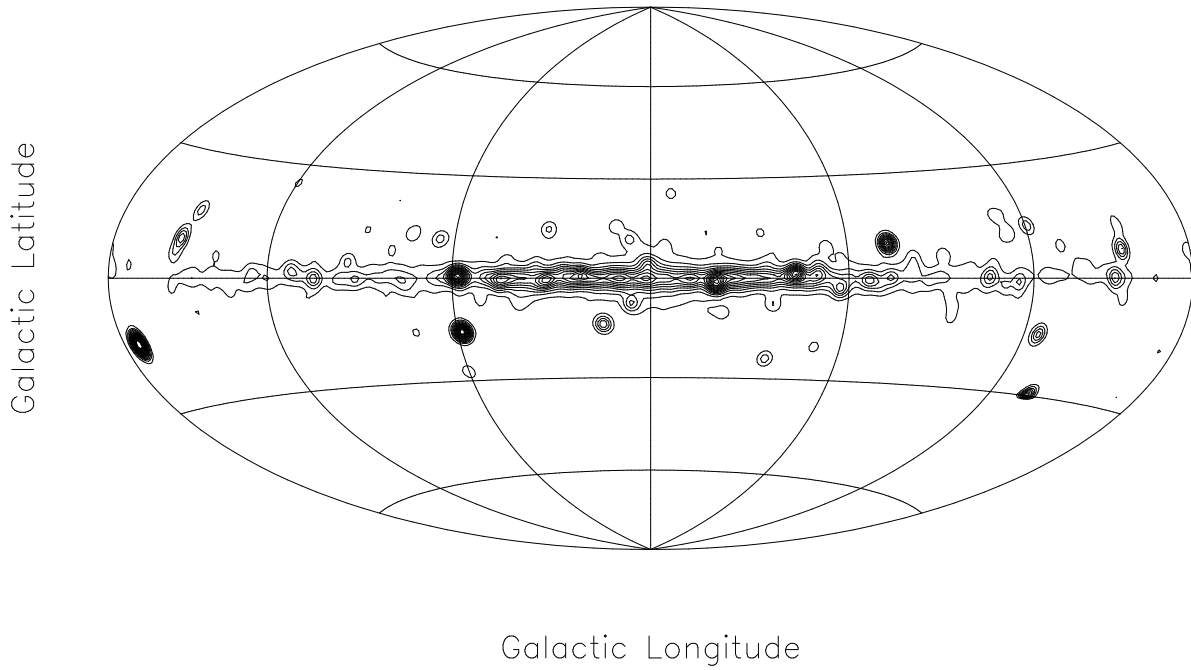


Fig. 1.— Contour plot of simulated intensity using an all-sky projection with a contour interval of $1.57 \times 10^{-5} \gamma \text{ cm}^{-2} \text{ s}^{-1}$. This plot is to be compared to the observed map of Oberlack et al. (1996).

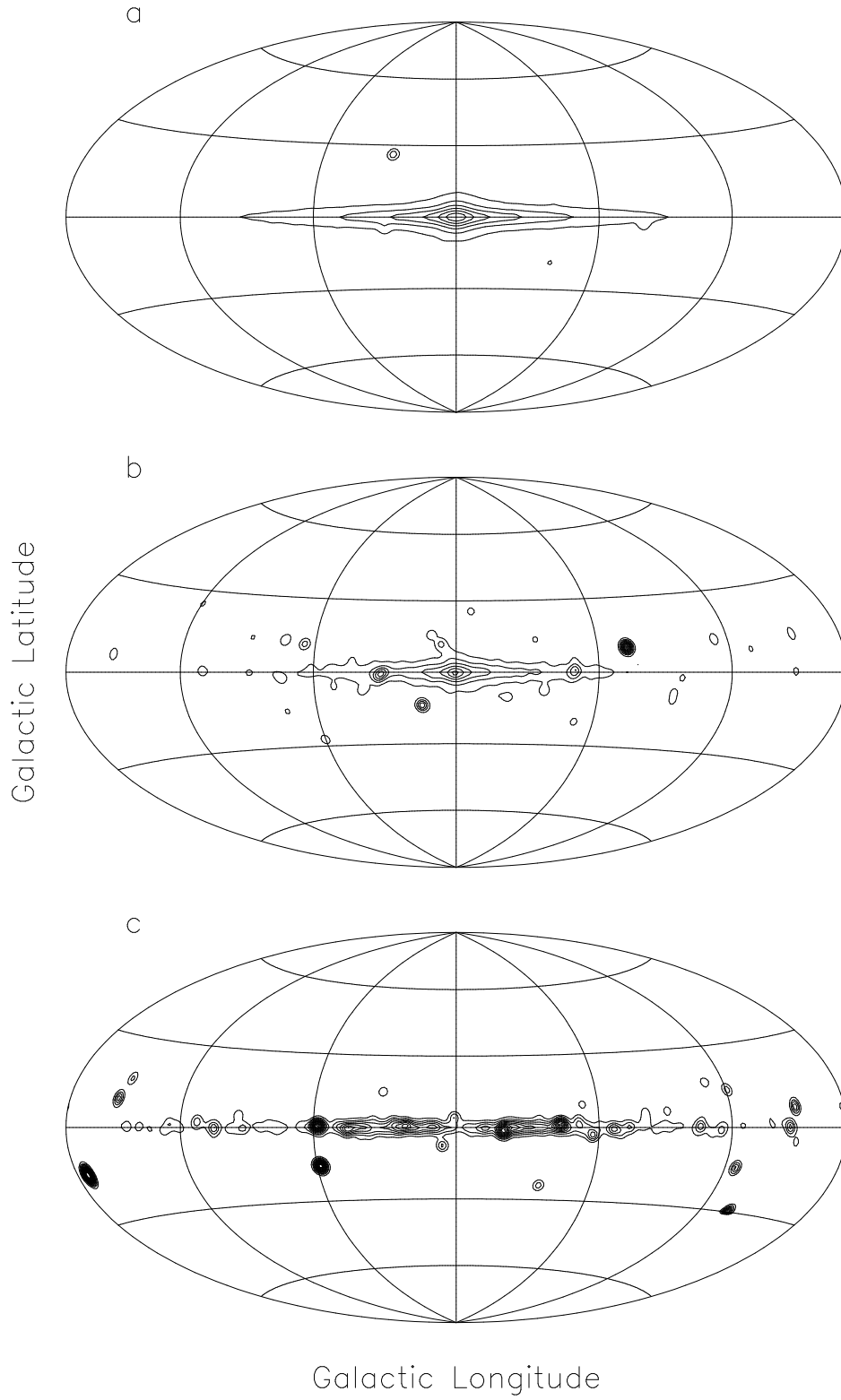


Fig. 2.— Intensities of model components in Figure 1 plotted with contours of $1.57 \times 10^{-5} \gamma \text{ cm}^{-2} \text{ s}^{-1}$. These include, a. the smooth component (novae and low-mass AGB stars) multiplied by 10, b. high-mass AGB stars, and c. objects with massive star progenitors (SNe and W-R stars).

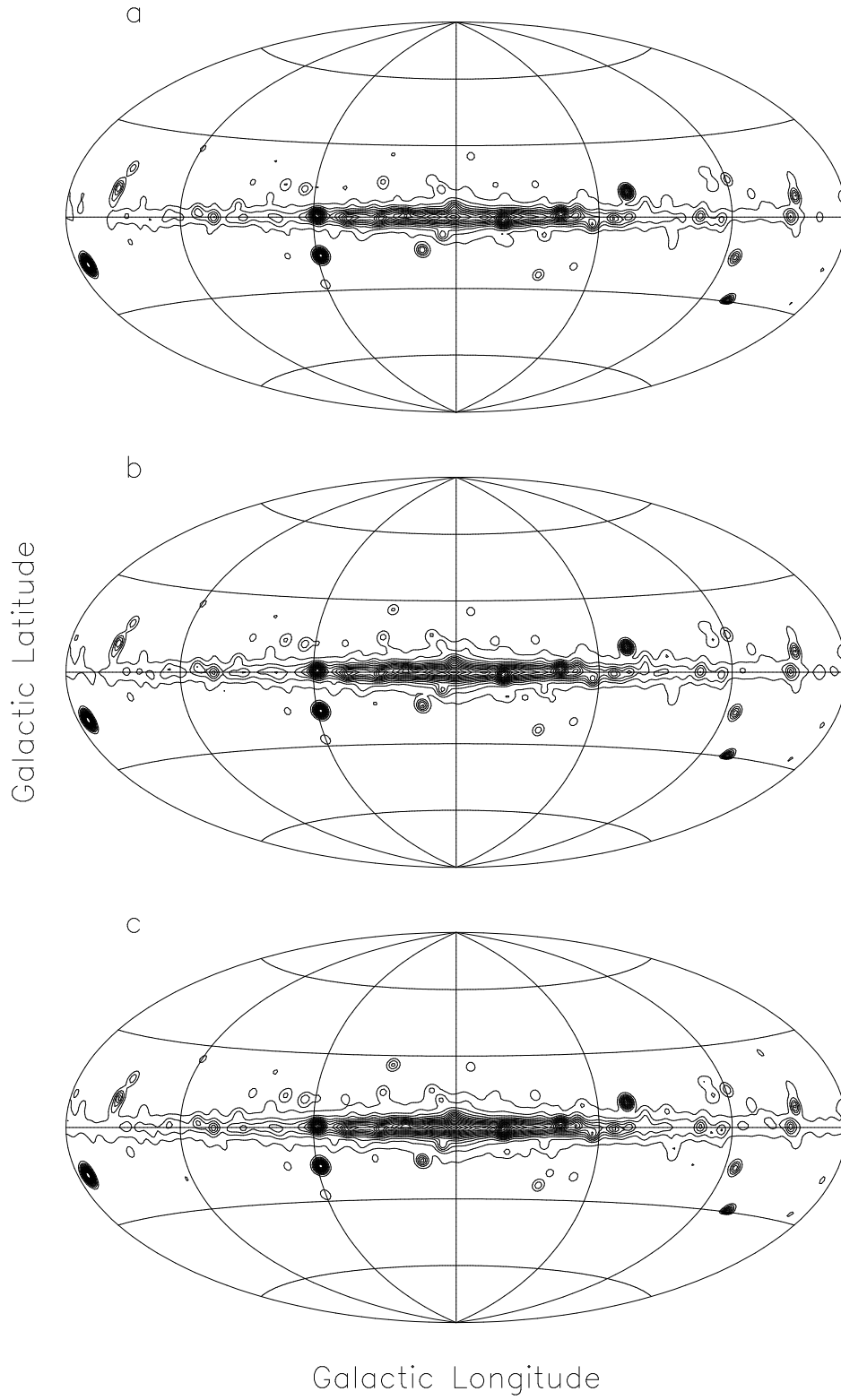


Fig. 3.— Contour plot of simulated intensity using $1.57 \times 10^{-5} \gamma \text{ cm}^{-2} \text{ s}^{-1}$ contours with a. 4 times, b. 8 times, c. 12 times the smooth source component in Figure 1.